NASA TECHNICAL NOTE

NASA TN D-5660

c. 1

EXPERIMENTAL PRESTON TUBE AND LAW-OF-THE-WALL STUDY OF TURBULENT SKIN FRICTION ON AXISYMMETRIC BODIES AT SUPERSONIC SPEEDS

by Jerry M. Allen

Langley Research Center
Langley Station, Hampton, Va.

NATIONAL AERONAUTICS AND SPACE ADMINISTRATION • WASHINGTON, D. C. • FEBRUARY 1970

1. Report No. NASA TN D-5660	2. Government Accession No.	3. Recipient's Catalog No.
4. Title and Subtitle EXPERIMENTAL PRESTON TUBE AND LAW-OF-THE-WALL STUDY OF TURBULENT SKIN FRICTION ON AXISYMMETRIC BODIES AT SUPERSONIC SPEEDS		5. Report Date February 1970 6. Performing Organization Code
7. Author(s) Jerry M. Allen		8. Performing Organization Report No. L-6686 10. Work Unit No. 720-01-11-02-23
9. Performing Organization Name and Address NASA Langley Research Center Hampton, Va. 23365		11. Contract or Grant No. 13. Type of Report and Period Covered Technical Note
12. Sponsoring Agency Name and Address National Aeronautics and Space Administration Washington, D.C. 20546		14. Sponsoring Agency Code

15. Supplementary Notes

16. Abstract

An experimental Preston tube study has been conducted in the turbulent boundary layer of a Haack-Adams body of revolution with a fineness ratio of 10 at free-stream Mach numbers of 2.50 to 4.50 and a free-stream Reynolds number, based on body length, of 9.15×10^6. The agreement between the Preston tube measurements and theoretical calculations of skin friction is good at the lower Mach numbers but becomes progressively worse at the higher Mach numbers.

Integration of the Preston tube skin-friction distributions over the body surface resulted in average skin-friction coefficients which were, at all Mach numbers, considerably below the values obtained from the difference between measured total drag and wave drag.

Law-of-the-wall skin-friction values were obtained from velocity profiles taken on the same Haack-Adams body and from profiles given in literature on a parabolic-arc body of revolution (NACA RM-10) and two slender cones. The skin-friction results were similar to those obtained from the Preston tube surveys at comparable Mach numbers; that is, the results show good agreement with theory over the rearward part of the bodies but become higher than theory as the nose of the body is approached.

17. Key Words Suggested by Author(s) Skin friction Preston tube Law of the wall Body of revolution	18. Distribution Statement Unclassified – Unlimited		
19. Security Classif. (of this report) Unclassified	20. Security Classif. (of this page) Unclassified	21. No. of Pages 27	22. Price* $3.00

*For sale by the Clearinghouse for Federal Scientific and Technical Information Springfield, Virginia 22151

EXPERIMENTAL PRESTON TUBE AND LAW-OF-THE-WALL STUDY OF TURBULENT SKIN FRICTION ON AXISYMMETRIC BODIES AT SUPERSONIC SPEEDS

By Jerry M. Allen
Langley Research Center

SUMMARY

An experimental Preston tube study has been conducted in the turbulent boundary layer of a Haack-Adams body of revolution with a fineness ratio of 10 at free-stream Mach numbers of 2.50 to 4.50 and a free-stream Reynolds number, based on body length, of 9.15×10^6. The agreement between the Preston tube measurements and theoretical calculations of skin friction is good at the lower Mach numbers but becomes progressively worse at the higher Mach numbers.

Integration of the Preston tube skin-friction distributions over the body surface resulted in average skin-friction coefficients which were, at all Mach numbers, considerably below the values obtained from the difference between measured total drag and wave drag.

Law-of-the-wall skin-friction values were obtained from velocity profiles taken on the same Haack-Adams body and from profiles given in literature on a parabolic-arc body of revolution (NACA RM-10) and two slender cones. The skin-friction results were similar to those obtained from the Preston tube surveys at comparable Mach numbers; that is, the results show good agreement with theory over the rearward part of the bodies but become higher than theory as the nose of the body is approached.

INTRODUCTION

The most direct method of testing the validity of Preston tube calibrations or law-of-the-wall theories is to compare the skin-friction results calculated from these methods with direct skin-friction measurements. In flow over a flat plate, the direct skin-friction measurements can be obtained with floating-element skin-friction balances so that the comparisons can be made relatively easily. (See refs. 1 to 3, for example.) In flow over a nonflat plate, however, floating-element-balance measurements are not convenient because the balance sensing element must match the body curvature, which generally

requires a different balance for each measuring station; hence, the motivation exists for comparison with other indirect techniques.

Both the Preston tube and law-of-the-wall methods use pressure measurements taken in the logarithmic part of the boundary layer, which is reported to be insensitive to changes in pressure gradient in incompressible flow. (See ref. 4.) That is, although pressure gradient affects the local skin friction, other parameters in the logarithmic law are affected in a manner to keep the law unchanged in the lower part of the boundary layer. Therefore, the law should yield correct skin-friction results in incompressible pressure-gradient flow, and by analogy the compressible law might be expected to do the same under pressure-gradient conditions.

This study was conducted to test the compressible Preston tube and law-of-the-wall methods in axisymmetric flow. Because of the difficulty in obtaining direct local skin-friction measurements in axisymmetric flow, theoretical calculations and total drag measurements were used as a basis of comparison.

The test model used in this study was a Haack-Adams body of revolution with a fineness ratio of 10 on which Preston tube and velocity-profile data were obtained at seven longitudinal locations. Local skin-friction values were calculated directly from the Preston tube measurements and somewhat more indirectly from the velocity profiles by using the law-of-the-wall theories. In addition, law-of-the-wall skin-friction results were obtained from the velocity profiles published in reference 5 which were taken on a slender body of revolution (NACA RM-10) and on two slender cones.

SYMBOLS

a	speed of sound
C_F	average skin-friction coefficient, $D_F/q_\infty S$
C_f	local skin-friction coefficient, τ_w/q_e
D_F	friction drag force
d	outside diameter of probe tip
l	model length
M	Mach number, u/a

p	static pressure
$p_{t,2}$	total pressure behind normal shock wave
q	dynamic pressure, $\frac{\gamma}{2} pM^2$
R	unit Reynolds number, $\rho_e u_e / \mu_e$
R_l	Reynolds number based on body length, $\rho_e u_e l / \mu_e$
R_x	Reynolds number based on streamwise coordinate, $\rho_e u_e x / \mu_e$
R_y	Reynolds number based on normal coordinate, $\rho_e u_e y / \mu_e$
r	body radius
S	wetted area
T	absolute temperature
u	velocity in x-direction
x	streamwise coordinate
y	normal coordinate
γ	ratio of specific heats
μ	absolute viscosity
ρ	density
σ	scaling parameter in Baronti-Libby transformation theory
τ	shearing stress

Subscripts:

aw	adiabatic wall

BL	determined by Baronti-Libby method
e	local conditions just outside boundary layer
FS	determined by Fenter-Stalmach method
HK	determined by Hopkins-Keener method
max	maximum
t	free stream stagnation
w	wall
∞	free stream

A bar over a symbol represents a transformed quantity.

APPARATUS AND TESTS

Wind Tunnel

This study was conducted in air in the high-speed test section of the Langley Unitary Plan wind tunnel described in reference 6. This variable-pressure, continuous-flow tunnel has an asymmetric sliding-block nozzle that permits a continuous variation in the test-section Mach number from 2.30 to 4.63. The nominal operating stagnation temperature is between 339° and 353° K. The test section is approximately 1.22 meters wide by 1.22 meters high by 2.13 meters long.

Model

A Haack-Adams body of revolution with a fineness ratio of 10 constructed of aluminum was used as the test model. This model was one of the six bodies used in reference 7. A sketch of the model, the model profile equation, and a list of model coordinates can be found in table I. The model is 91.440 cm long and has a ratio of base cross-sectional area to maximum cross-sectional area of 0.532. A single row of static-pressure orifices is located along the length of the body; at the 17.780- and 66.040-cm stations, orifices were located 90° apart around the body. The model was sting mounted from the rear.

Tests and Instrumentation

The free-stream test conditions are summarized in the following table:

M_∞	T_t, ^oK	R_∞, cm^{-1}	$R_{l,\infty}$
2.50	339	0.1×10^6	9.15×10^6
2.96	339	.1	9.15
3.95	353	.1	9.15
4.50	353	.1	9.15

Approximately 30 minutes was allowed between the establishment of supersonic flow and the recording of experimental data to insure that pressure and temperature conditions in the test section had reached equilibrium. For these test conditions, the conductive and radiative heat transfer from the model should be small compared with the aerodynamic heating; hence, equilibrium model temperatures were assumed to be adiabatic.

Preston tube surveys were made at seven longitudinal stations (table I) for each of the test Mach numbers. Velocity-profile surveys were obtained for $M_\infty = 2.96$. Model static-pressure distributions were obtained for each of the test Mach numbers.

The Preston tube consisted of a stainless-steel tube with an outside diameter of 0.71 mm $\left(\frac{\text{Inside diameter}}{\text{Outside diameter}} = 0.58\right)$ connected to a shaft which ran through the tunnel sidewall. (See fig. 1.) The tube position normal to the model center line was controlled manually from outside the tunnel by a traversing mechanism connected to the probe shaft. The model-surface position was determined by electrical contact between the model and the probe, and the distance above the model surface (needed for the velocity-profile surveys) was determined from the surface contact point and a dial indicator connected to the probe shaft. The different survey stations were reached by moving the model in the streamwise direction.

Preston tube data were taken with the probe in contact with the model surface. The probe was then traversed to the edge of the boundary layer (determined by negligible change in impact pressure), and a second data point was recorded in order to determine local free-stream conditions.

The impact-pressure surveys were obtained by replacing the Preston tube with a small, flattened boundary-layer probe (fig. 1) and recording 10 to 15 data points through the boundary layer instead of just the wall and local free-stream points.

The pressures from these impact probes were sensed by three pressure transducers, the ranges of which were 0 to 0.34, 0 to 0.68, and 0 to 1.02 atmospheres (1 atm = 1.013×10^5 N/m2). In this manner the gage having the smallest possible range could be used for maximum accuracy.

The impact probes were bent approximately parallel to the model surface at the first station. Because of the longitudinal curvature of the model, however, the impact surveys at the other stations were made with the probe at small angles to the local surface slope. The largest angle, occurring at station 6, was approximately 10°. A check run was made at station 6 with the probe bent parallel to the model at that station. A comparison of the two surveys revealed that the small angles at which the probe was inclined to the model had a negligible effect on the results of this test.

The model static pressures were measured by connecting the orifices to valves which were sampled in sequence by a single transducer. The static-pressure data were recorded with the model moved upstream of the impact probe to insure that no probe interference was present. Static-pressure distributions taken on the same model at the three lower Mach numbers are given in reference 7, in which the model was not moved upstream to obtain the data. Comparing the pressures recorded in the present study with those of reference 7 revealed that moving the model had a negligible effect on the static-pressure distributions.

All pressures were recorded at zero angle of attack, which was obtained by adjusting the model until the static pressures at the four circumferential orifices at the 17.780-cm station were balanced. The impact-pressure surveys were made along a ray 180° from the single row of static-pressure orifices. The static-pressure data were recorded without a transition strip on the model so that the static pressures measured near the nose of the model would not be influenced by the roughness elements. Boundary-layer transition was fixed near the nose for the impact-pressure surveys by placing a 0.32-cm-wide band of No. 60 carborundum grit 1.27 cm from the nose of the model. Static-pressure data were also recorded with the transition strip on the model to verify that the turbulent boundary layer did not affect the static-pressure distribution. The grit-on and grit-off static-pressure data were in excellent agreement over the entire length of the model except in the region immediately downstream of the transition strip. In this region, the transition strip caused a sharp decrease in pressure.

Examination of the velocity profiles obtained from the impact-pressure surveys revealed that the velocity-profile index at station 1 ($x/l = 0.1389$) was approximately 7; therefore the establishment of fully turbulent flow at the most forward station was substantiated. Both the static and the impact pressures were digitized and recorded on punched cards to expedite data reduction.

DATA REDUCTION

The static-pressure distributions obtained on the model are shown in figure 2. Impact pressures were combined with the appropriate static pressures to obtain values of local Mach number from the Rayleigh pitot formula:

$$\frac{p_{t,2}}{p} = \left(\frac{\gamma + 1}{2} M^2\right)^{\frac{\gamma}{\gamma-1}} \left(\frac{\gamma + 1}{2\gamma M^2 - \gamma + 1}\right)^{\frac{1}{\gamma-1}} \tag{1}$$

This procedure requires the usual assumption of constant static pressure across the boundary layer.

Velocity ratios are related to Mach number and temperature by

$$\frac{u}{u_e} = \frac{M}{M_e}\sqrt{\frac{T}{T_t}}\sqrt{\frac{T_{t,e}}{T_e}}\sqrt{\frac{T_t}{T_{t,e}}} \tag{2}$$

where

$$\left.\begin{aligned} \frac{T_t}{T} &= 1 + \frac{\gamma - 1}{2} M^2 \\ \text{and} \\ \frac{T_{t,e}}{T_e} &= 1 + \frac{\gamma - 1}{2} M_e^2 \end{aligned}\right\} \tag{3}$$

For the data obtained in this investigation, velocity ratios were calculated by assuming that the total-temperature distribution through the boundary layer was constant and equal to $T_{t,e}$. This assumption used with equations (2) and (3) results in

$$\frac{u}{u_e} = \frac{M}{M_e}\sqrt{\frac{1 + \frac{\gamma - 1}{2} M_e^2}{1 + \frac{\gamma - 1}{2} M^2}} \tag{4}$$

This constant-total-temperature assumption is, of course, only an approximation to the true temperature distribution and has its largest inaccuracy near the wall since the total temperature must approach recovery temperature in this region. For the highest Mach number in this study ($M_\infty = 4.50$), the recovery temperature is approximately 10 percent lower than the free-stream total temperature. If equation (2) had been used instead of equation (4), the velocity ratios in the immediate vicinity of the wall would have been

approximately 5 percent lower. These lower velocity ratios would have resulted in a decrease in skin-friction coefficients of about 10 percent in the immediate wall region from calculations using the equations presented and discussed in the next paragraph. It was believed, however, that no increase in accuracy would have resulted from use of a more accurate temperature distribution through the boundary layer since the constants in these equations were themselves derived from data in which this constant-total-temperature assumption had been made; hence equation (4) was used in this paper to calculate velocity ratios.

Local skin-friction coefficients were calculated from the experimental data by using the Preston tube calibration of Hopkins and Keener (ref. 1), the law-of-the-wall theory of Baronti and Libby (ref. 2), and the method of Fenter and Stalmach (ref. 8) which is used both as a Preston tube calibration and as a law-of-the-wall theory. The inputs required for these methods are the local flow conditions in the form of M_e, R, T_t, and T_w/T_e and the experimental data in the form of u/u_e and y. In the Preston tube calibrations, y is simply half the probe diameter. The equations (in the notation of the present paper) obtained from reference 3 are as follows:

Hopkins-Keener equation:

$$C_f = \frac{\left(\frac{u}{u_e}\right)^{1.767}\left(0.55 + 0.035M_e^2 + 0.45\frac{T_w}{T_e}\right)^{0.466}\left(T_t + 199 + 39.8M_e^2\right)^{0.233}}{25.7\left\{1 + 0.2M_e^2\left[1 - \left(\frac{u}{u_e}\right)^2\right]\right\}^{0.884} R_y^{0.233}\left(0.55T_t + 0.035T_tM_e^2 + 0.45T_t\frac{T_w}{T_e} + 199 + 39.8M_e^2\right)^{0.233}} \tag{5}$$

Fenter-Stalmach equation:

$$\frac{\sqrt{5 + M_e^2}}{M_e\sqrt{\frac{T_w}{T_e}}}\sin^{-1}\left(\frac{M_e}{\sqrt{5 + M_e^2}}\frac{u}{u_e}\right) = \sqrt{C_f}\left\{2.03\log_{10}\left[\frac{R_y^2C_f}{\left(\frac{T_w}{T_e}\right)^{2.536}}\right] + 2.99\right\} \tag{6}$$

and Baronti-Libby equations:

$$\frac{u}{u_e} = 1.718\sqrt{C_f}\log_e\left\{5.3\sqrt{C_f}\left(\frac{\sigma\mu_e}{\bar{\mu}}\right)R\int_0^y\left[\frac{T_w}{T_e} + \left(1 + 0.2M_e^2 - \frac{T_w}{T_e}\right)\frac{u}{u_e} - 0.2M_e^2\left(\frac{u}{u_e}\right)^2\right]^{-1}dy\right\} \tag{7}$$

and

$$C_f = \sqrt{\frac{T_w}{T_e}} \frac{T_t + 199 + 39.8M_e^2}{\frac{T_w}{T_e} T_t + 199 + 39.8M_e^2} \frac{\sigma\mu_e}{\bar{\mu}} \bar{C}_f \tag{8}$$

where

$$\frac{\sigma\mu_e}{\bar{\mu}} = \frac{\left[\frac{T_w}{T_e} T_t + \left(1 + 0.2M_e^2 - \frac{T_w}{T_e}\right) T_t \sqrt{\bar{C}_f}\, 7.50 - 11.24M_e^2 \bar{C}_f T_t + 199 + 39.8M_e^2\right]\left[\frac{T_w}{T_e} + 3.75\left(1 + 0.2M_e^2 - \frac{T_w}{T_e}\right)\sqrt{\bar{C}_f} - 3.75M_e^2 \bar{C}_f\right]}{\left[\frac{T_w}{T_e} + 7.50\left(1 + 0.2M_e^2 - \frac{T_w}{T_e}\right)\sqrt{\bar{C}_f} - 11.24M_e^2 \bar{C}_f\right]^{2.5} \left(T_t + 199 + 39.8M_e^2\right)} \tag{9}$$

The Hopkins-Keener equation is directly solvable for C_f, whereas the Fenter-Stalmach equation requires iteration. In the Baronti-Libby method, equations (7) and (9) are used to solve, by iteration, for $\bar{C}_f$ which is used in equation (8) to solve for C_f. The technique for using these equations with Preston tube measurements is simply to calculate, from the Hopkins-Keener and Fenter-Stalmach equations, skin-friction values for each data point.

The law-of-the-wall technique, however, usually requires an interpolation process, which can best be described with the aid of figure 3. This figure, an illustration of the interpolation process, contains the experimental velocity profile taken at station 5 on the test model. The plane in which this profile is plotted is required by the Baronti-Libby law. A different plane would have been used if the example had illustrated the Fenter-Stalmach law, but the interpolation process would have been the same.

Also shown in figure 3 are the curves calculated from the Baronti-Libby equations. Each curve represents a constant value of skin friction; the C_f increment between the curves is approximately 0.0001 (which, for a Mach number of 2.96, is an increment of exactly 0.0002 in $\bar{C}_f$). The value of wall skin friction is found from the experimental data and the Baronti-Libby curves by interpolating between the curves in the range where the data become approximately parallel to the curves. This interpolated value of $\bar{C}_f$ is shown by the dashed line in figure 3.

This technique requires a separate plot for each local free-stream Mach number and becomes very tedious when a large number of profiles are involved. The same result can be obtained without plotting by using the computer calculation technique described in reference 3. This technique was used to obtain the law-of-the-wall skin-friction results presented in this paper and is described briefly as follows.

The computer program is used to calculate skin-friction values for each point in the profiles by using the Baronti-Libby and Fenter-Stalmach equations. The correct wall skin-friction values were found by observing the trend of C_f through the profile and

noting where C_f became relatively constant. The C_f values becoming constant is equivalent to the data being parallel to the law-of-the-wall curves in the plotting technique. The correct wall skin-friction value is then chosen from this constant-skin-friction region.

Total skin-friction values were obtained by integrating the local skin-friction distributions over the wetted area of the body as follows:

By definition

$$D_F = \int_0^{S_{max}} \tau_w \, dS \tag{10}$$

Substituting the definitions

$$\left.\begin{aligned} C_f &\equiv \frac{\tau_w}{q_e} \\ \text{and} \\ C_F &\equiv \frac{D_F}{q_\infty S_{max}} \end{aligned}\right\} \tag{11}$$

into equation (10) yields

$$C_F = \int_0^1 \frac{q_e}{q_\infty} C_f d\left(\frac{S}{S_{max}}\right) \tag{12}$$

RESULTS AND DISCUSSION

Skin Friction on Haack-Adams Body From Preston Tube Survey

The local skin-friction distributions obtained from the Preston tube surveys on the Haack-Adams body are shown in figure 4 and are listed in table II. The theory used for comparison with the data is that of reference 9. For all four Mach numbers, the Hopkins-Keener results are higher near the nose of the model than the Fenter-Stalmach results but are lower over the rearward part of the body. It should be emphasized that at each model station both the Hopkins-Keener and Fenter-Stalmach skin-friction values were obtained from the same experimental measurements; thus, the disagreement between the two values is the result of differences in the calibrations.

The general trend of the data, except near the nose and base of the model, seems to follow the theory, but the absolute agreement becomes progressively worse with increasing Mach number. The rapidly increasing experimental skin-friction values near the nose of the body could be caused by several factors:

(1) The thin boundary layer in this region results in a ratio of probe diameter to boundary-layer thickness which could be too large to give accurate Preston tube measurements.

(2) If boundary-layer transition did not occur for a short distance downstream of the trips, the skin-friction values near the nose would tend to be higher than where turbulent flow was established at the nose.

(3) It can be seen from figure 2 that the region of largest pressure gradient on this model occurs near the nose. If Preston tube calibrations do not properly account for pressure gradients, the most inaccurate results would be in this nose region.

Figure 2 also shows that a region of slight adverse pressure gradient occurs near the base of the model. The theory predicts a pronounced decrease in skin friction in this region, which seems reasonable since an adverse pressure gradient promotes boundary-layer separation and the skin friction must decrease to zero at separation. The data, however, do not follow this trend. In fact, at the higher Mach numbers skin friction tends to increase near the base.

Shown in figure 4 are flat-plate skin-friction curves calculated from the axisymmetric theory of reference 9 by using the free-stream values of Mach number and Reynolds number. The level of the Preston tube measurements appears to be more accurately predicted by the flat-plate theory than by the axisymmetric theory. If these theory curves are accurate, it appears that the Preston tube calibrations do not properly account for the effects of pressure gradient and axisymmetric flow on skin friction.

Also shown in figure 4 are average skin-friction values for each of the Mach numbers. The theoretical average skin-friction values were obtained from equation (12) simply by integrating the theoretical local skin-friction distributions over the surface wetted area. The average flat-plate skin-friction values were similarly obtained by integration of the local flat-plate skin-friction distributions over a flat surface, the length of which was equal to the length of the model.

The average skin-friction values calculated from the Preston tube measurements were obtained by integrating the experimental local skin-friction distributions shown in figure 4 over the surface wetted area. The distributions were extrapolated from the first station to the nose of the body by assuming conical flow in this region and calculating the skin-friction distributions from slender-cone theory. Also, the distributions between the rear station and the end of the body were obtained by extrapolating the experimental distributions to the end of the body.

Figure 4 also shows the average skin-friction values obtained from reference 7 by determining the difference between the total drag of the body, measured with an internally

mounted strain-gage balance, and the experimental wave drag, obtained by integration of the pressure distribution over the model surface. Trip drag was assumed to be negligible. Reference 7 did not contain any data at $M_\infty = 4.50$; therefore, the value of C_F for this Mach number was obtained by extrapolating the data from the other three Mach numbers.

Figure 4 shows that the average skin friction obtained by this indirect measurement was higher than that obtained from theory or from integration of the Preston tube results. One possible explanation for this discrepancy is the fact that the model used in this test is a low-wave-drag body. In making force balance measurements with an internally mounted gage, a correction is usually applied to the measured drag to account for the drag forces felt by the base and internal parts of the model. On a general model, this correction term is a small part of the measured drag. Because the measured drag on this model was small, however, the correction term was a significant part of the total drag. It was, in fact, of the same order as the skin-friction drag. Any appreciable errors in the calculation of this correction term, therefore, would result in a similar error being introduced into the average skin-friction coefficient. As a result of the Preston tube and flat-plate-theory local skin-friction distributions being in reasonable agreement, the average skin-friction values are in reasonable agreement. It is interesting to note that comparable results were obtained in reference 5 on a similar body.

Skin Friction Determined From Law-of-the-Wall Surveys

Haack-Adams body.- Velocity profiles were obtained on the Haack-Adams body at all seven stations at $M_\infty = 2.96$. Local skin-friction coefficients were calculated from these profiles by using the law-of-the-wall techniques of Baronti and Libby (ref. 2) and Fenter and Stalmach (ref. 8), and the results are shown in figure 5 and listed in table III. Over the rearward part of the body, the two methods are in good agreement with each other and with the theory presented in reference 9. This good agreement between the Baronti-Libby and Fenter-Stalmach methods was also reported in reference 3 in which the results from a large number of flat-plate profiles were analyzed. Figure 5 shows also that the skin-friction values obtained by law-of-the-wall methods were generally higher than those obtained by the Preston tube methods.

NACA RM-10.- Local skin-friction values were also determined by these law-of-the wall techniques from velocity profiles presented in reference 5. The models used were two slender cones and a slender parabolic-arc body of revolution (NACA RM-10). The law-of-the wall results on the RM-10 are shown in figure 6. The theory curves were calculated by the same method used for the theory calculation for the Haack-Adams body – that of reference 9.

Also shown in figure 6 are experimental results, obtained from reference 5, derived from momentum-thickness measurements by using a modified Reshotko and Tucker equation. The overall results are similar to those obtained on the Haack-Adams body at the lower Mach numbers; good agreement is shown among the different methods of obtaining local skin friction.

Slender cones.- Figure 7 shows the results obtained from the velocity profiles presented in reference 5 for two slender cones. The flat-plate theory of Spalding and Chi (ref. 10) and slender-cone theory (approximately 18 percent above flat-plate theory) are shown for comparison, as are the experimental results obtained from reference 5, which were derived from momentum-thickness measurements (fig. 7(c)).

Good agreement is seen between the law-of-the-wall results and theory at the higher Reynolds numbers, but the law-of-the-wall results are higher than theory at the lower Reynolds numbers. The same trend was noted in the law-of-the-wall results of the Haack-Adams body and the NACA RM-10 but is not present in the momentum-thickness results of figure 7(c). Since the static pressure is constant over the surface of these cones, the increasing skin-friction values near the nose are not caused by pressure-gradient effects on the Preston tube calibration.

CONCLUDING REMARKS

An experimental Preston tube and law-of-the-wall study has been conducted in the turbulent boundary layer of a Haack-Adams body of revolution with a fineness ratio of 10 at free-stream Mach numbers of 2.50 to 4.50 and a free-stream Reynolds number, based on body length, of 9.15×10^6. The conclusions to be drawn from this study necessarily suffer from the lack of a solid, reliable base – preferably direct measurements – with which to compare the indirect methods of determining local skin friction on a pressure-gradient body of revolution. Since the results of these several indirect methods did not agree over the entire length of the body, it is impossible from the present data to assess the overall accuracy of the Preston tube and law-of-the-wall methods under these flow conditions. Several specific observations, however, can be made about the results of the present study:

The agreement between the Preston tube measurements and theoretical calculations of skin friction is good at the lower Mach numbers but becomes progressively worse at the higher Mach numbers.

Integration of the Preston tube skin-friction distributions over the body surface results in average skin-friction coefficients which are, at all Mach numbers, considerably below the values obtained from the difference between measured total drag and wave drag.

Law-of-the-wall skin-friction results obtained from velocity profiles taken on the same Haack-Adams body of revolution are generally higher than those obtained from the Preston tube surveys at the same Mach number. Results obtained from velocity profiles given in literature for a parabolic-arc body of revolution (NACA RM-10) and two slender cones are similar to those obtained from the Preston tube surveys at comparable Mach numbers. These results show good agreement with theory over the rearward part of the body but become higher than theory as the nose of the body is approached.

Langley Research Center,
National Aeronautics and Space Administration,
Langley Station, Hampton, Va., December 3, 1969.

REFERENCES

1. Hopkins, Edward J.; and Keener, Earl R.: Study of Surface Pitots for Measuring Turbulent Skin Friction at Supersonic Mach Numbers – Adiabatic Wall. NASA TN D-3478, 1966.

2. Baronti, Paolo O.; and Libby, Paul A.: Velocity Profiles in Turbulent Compressible Boundary Layers. AIAA J., vol. 4, no. 2, Feb. 1966, pp. 193-202.

3. Allen, Jerry M.: Use of Baronti-Libby Transformation and Preston Tube Calibrations To Determine Skin Friction From Turbulent Velocity Profiles. NASA TN D-4853, 1968.

4. Ludwieg, H.; and Tillmann, W.: Investigations of the Wall-Shearing Stress in Turbulent Boundary Layers. NACA TM 1285, 1950.

5. Allen, Jerry M.; and Monta, William J.: Turbulent-Boundary-Layer Characteristics of Pointed Slender Bodies of Revolution at Supersonic Speeds. NASA TN D-4193, 1967.

6. Anon.: Manual for Users of the Unitary Plan Wind Tunnel Facilities of the National Advisory Committee for Aeronautics. NACA, 1956.

7. Harris, Roy V., Jr.; and Landrum, Emma Jean: Drag Characteristics of a Series of Low-Drag Bodies of Revolution at Mach Numbers From 0.6 to 4.0. NASA TN D-3163, 1965.

8. Fenter, Felix W.; and Stalmach, Charles J., Jr.: The Measurement of Local Turbulent Skin Friction at Supersonic Speeds by Means of Surface Impact Pressure Probes. DRL-392, CM-878 (Contract NOrd-16498), Univ. of Texas, Oct. 21, 1957.

9. Jackson, Charlie M., Jr.; and Smith, Rudeen S.: A Method for Determining the Total Drag of a Pointed Body of Revolution in Supersonic Flow With Turbulent Boundary Layer. NASA TN D-5046, 1969.

10. Spalding, D. B.; and Chi, S. W.: The Drag of a Compressible Turbulent Boundary Layer on a Smooth Flat Plate With and Without Heat Transfer. J. Fluid Mech., vol. 18, pt. 1, Jan. 1964, pp. 117-143.

TABLE I.- MODEL INFORMATION

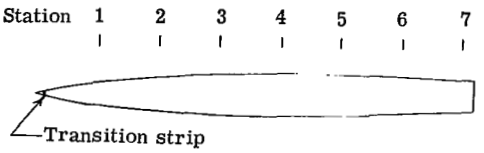

Model profile equation

$$\frac{r}{r_{max}} = \left\{0.70700\left[1 - \left(\frac{2x}{l} - 1\right)^{2.0}\right]^{1.5} + 0.16934\left(\frac{2x}{l} - 1\right)\left[1 - \left(\frac{2x}{l} - 1\right)^{2.0}\right]^{0.5} + 0.16934 \cos^{-1}\left(1 - \frac{2x}{l}\right)\right\}^{0.5}$$

where

$$r_{max} = 4.572 \text{ cm}$$

and

$$l = 91.44 \text{ cm}$$

Station	x/l
1	0.1389
2	.2778
3	.4167
4	.5556
5	.6944
6	.8333
7	.9722

Model coordinates

x, cm	r, cm	x, cm	r, cm
0	0	38.100	4.308
.254	.137	40.640	4.392
.508	.234	43.180	4.458
.762	.320	45.720	4.511
1.016	.396	48.260	4.547
1.270	.470	50.800	4.567
1.524	.538	53.340	4.572
1.778	.602	55.880	4.562
2.032	.663	58.420	4.539
2.286	.724	60.960	4.501
2.540	.782	63.500	4.450
3.810	1.049	66.040	4.384
5.080	1.290	68.580	4.305
7.620	1.715	71.120	4.216
10.160	2.085	73.660	4.115
12.700	2.413	76.200	4.003
15.240	2.710	78.740	3.884
17.780	2.974	81.280	3.757
20.320	3.216	83.820	3.630
22.860	3.432	85.090	3.566
25.400	3.630	86.360	3.508
27.940	3.800	87.630	3.452
30.480	3.955	88.900	3.401
33.020	4.089	90.170	3.358
35.560	4.206	91.440	3.335

TABLE II.- PRESTON TUBE DATA FOR HAACK-ADAMS BODY

[d = 0.71 mm; l = 91.44 cm; $R_\infty = 0.1 \times 10^6$ cm^{-1}; $T_w/T_{aw} \approx 1$]

Station	M_∞	M_e	T_t, ^oK	R_e, cm^{-1}	M	u/u_e	$C_{f,HK}$	$C_{f,FS}$	x/l
1	2.50	2.3632	339	0.1047×10^6	1.4788	0.7594	0.002894	0.002801	0.1389
2		2.4655		.1013	1.3476	.6969	.002323	.002356	.2778
3		2.5290		.0994	1.3295	.6822	.002194	.002250	.4167
4		2.5625		.0972	1.2504	.6478	.001941	.002044	.5556
5		2.5956		.0961	1.2117	.6288	.001805	.001928	.6944
6		2.5761		.0941	1.1194	.5928	.001595	.001747	.8333
7		2.4588		.0930	1.0400	.5700	.001505	.001666	.9722
1	2.96	2.8241	339	0.1081×10^6	1.6620	0.7609	0.002718	0.002583	0.1389
2		2.9649		.1052	1.5265	.7062	.002196	.002198	.2778
3		3.0264		.1016	1.4194	.6663	.001891	.001967	.4167
4		3.0456		.0977	1.3282	.6336	.001682	.001804	.5556
5		3.0716		.0955	1.2887	.6176	.001584	.001725	.6944
6		3.0771		.0937	1.2191	.5917	.001439	.001602	.8333
7		2.9442		.0928	1.1147	.5602	.001310	.001486	.9722
1	3.95	3.6568	353	0.1128×10^6	1.8219	0.7404	0.002213	0.002121	0.1389
2		3.9174		.1106	1.6384	.6805	.001685	.001742	.2778
3		4.0597		.1064	1.5440	.6487	.001462	.001576	.4167
4		4.1211		.1008	1.4421	.6166	.001287	.001447	.5556
5		4.1846		.0974	1.3890	.5983	.001191	.001373	.6944
6		4.2322		.0952	1.2313	.5456	.000954	.001163	.8333
7		3.9365		.0863	1.1496	.5258	.000948	.001171	.9722
1	4.50	4.1085	353	0.1163×10^6	1.8327	0.7217	0.001909	0.001872	0.1389
2		4.3658		.1096	1.6045	.6550	.001418	.001527	.2778
3		4.5879		.1064	1.4704	.6112	.001151	.001317	.4167
4		4.7776		.1042	1.3971	.5851	.001007	.001198	.5556
5		4.8637		.1011	1.2841	.5481	.000854	.001066	.6944
6		4.8626		.0961	1.1884	.5165	.000754	.000978	.8333
7		4.6040		.0868	1.1493	.5082	.000778	.001015	.9722

TABLE III.- VELOCITY-PROFILE DATA FOR HAACK-ADAMS BODY

$M_\infty = 2.96$; $R_\infty = 0.1 \times 10^6$ cm^{-1}; $T_t = 339^\circ$ K; $T_w/T_{aw} \approx 1$

Station 1		Station 2		Station 3	
$M_e = 2.832$		$M_e = 2.973$		$M_e = 3.038$	
$x/l = 0.1389$		$x/l = 0.2778$		$x/l = 0.4167$	
$R_e = 0.1089 \times 10^6$ cm^{-1}		$R_e = 0.1060 \times 10^6$ cm^{-1}		$R_e = 0.1027 \times 10^6$ cm^{-1}	
y, cm	u/u_e	y, cm	u/u_e	y, cm	u/u_e
0.0127	0.5865	0.0127	0.5434	0.0127	0.5055
.0254	.6181	.0381	.6846	.0508	.7025
.0381	.7416	.0635	.7889	.0889	.7830
.0635	.8503	.0889	.8307	.1270	.8223
.1143	.9319	.1651	.9000	.2159	.8859
.1651	.9807	.2413	.9564	.3429	.9533
.2159	.9981	.3175	.9881	.4699	.9897
.2667	1.0000	.3937	.9964	.5969	.9968
.3175	1.0000	.4699	.9981	.7239	.9991
.3683	.9983	.5461	.9990	.8509	1.0000
.4191	.9992	.6223	1.0000	.9779	.9984
$C_{f,BL} = 0.002739$		$C_{f,BL} = 0.002267$		$C_{f,BL} = 0.002082$	
$C_{f,FS} = 0.002892$		$C_{f,FS} = 0.002354$		$C_{f,FS} = 0.002094$	

Station 4		Station 5		Station 6		Station 7	
$M_e = 3.050$		$M_e = 3.072$		$M_e = 3.071$		$M_e = 2.935$	
$x/l = 0.5556$		$x/l = 0.6944$		$x/l = 0.8333$		$x/l = 0.9722$	
$R_e = 0.0983 \times 10^6$ cm^{-1}		$R_e = 0.0957 \times 10^6$ cm^{-1}		$R_e = 0.0933 \times 10^6$ cm^{-1}		$R_e = 0.0921 \times 10^6$ cm^{-1}	
y, cm	u/u_e	y, cm	u/u_e	y, cm	u/u_e	y, cm	u/u_e
0.0127	0.4414	0.0127	0.4154	0.0127	0.3980	0.0127	0.3895
.0508	.6462	.0635	.6691	.0762	.6678	.0889	.6489
.0889	.7452	.1143	.7414	.1397	.7321	.1651	.6973
.1270	.7827	.1651	.7803	.2032	.7702	.2413	.7544
.1905	.8258	.2159	.8105	.2667	.8033	.3175	.7879
.3175	.8966	.2667	.8367	.3302	.8334	.3937	.8204
.4445	.9483	.4699	.9199	.3937	.8572	.5207	.8626
.5715	.9829	.6731	.9745	.6477	.9329	.7747	.9290
.6985	.9962	.8763	.9966	.9017	.9823	1.0287	.9748
.8255	.9983	1.0795	.9990	1.1557	.9978	1.2827	.9963
.9525	.9990	1.2827	.9997	1.4097	.9991	1.5367	1.0000
1.0795	.9996	1.4859	1.0000	1.6637	1.0000	1.7907	.9969
1.2065	1.0000					2.0447	.9980
						2.2987	.9979
						2.5527	.9976
$C_{f,BL} = 0.001904$		$C_{f,BL} = 0.001767$		$C_{f,BL} = 0.001656$		$C_{f,BL} = 0.001568$	
$C_{f,FS} = 0.001905$		$C_{f,FS} = 0.001775$		$C_{f,FS} = 0.001652$		$C_{f,FS} = 0.001563$	

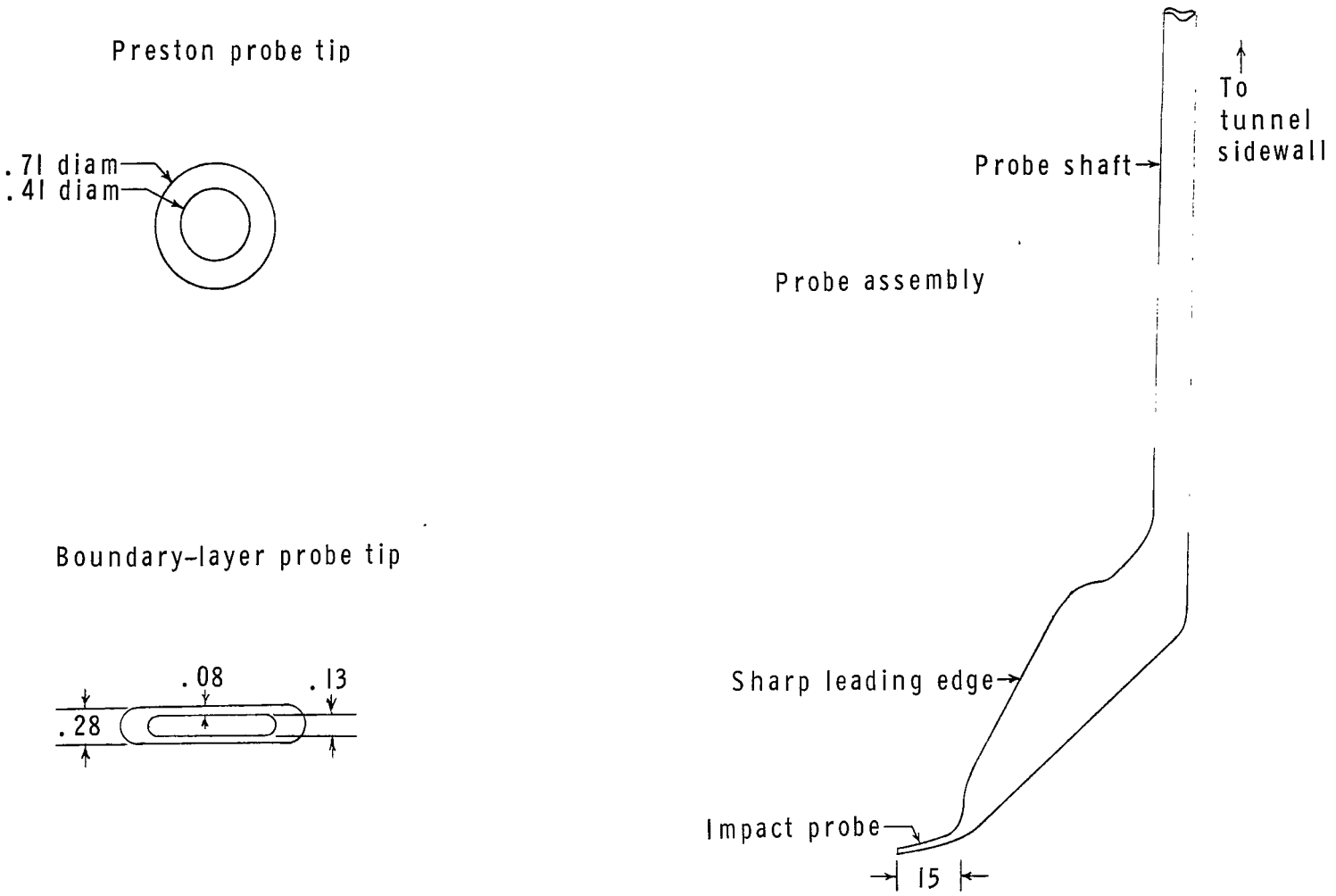

Figure 1.- Probe sketches. All dimensions are in millimeters.

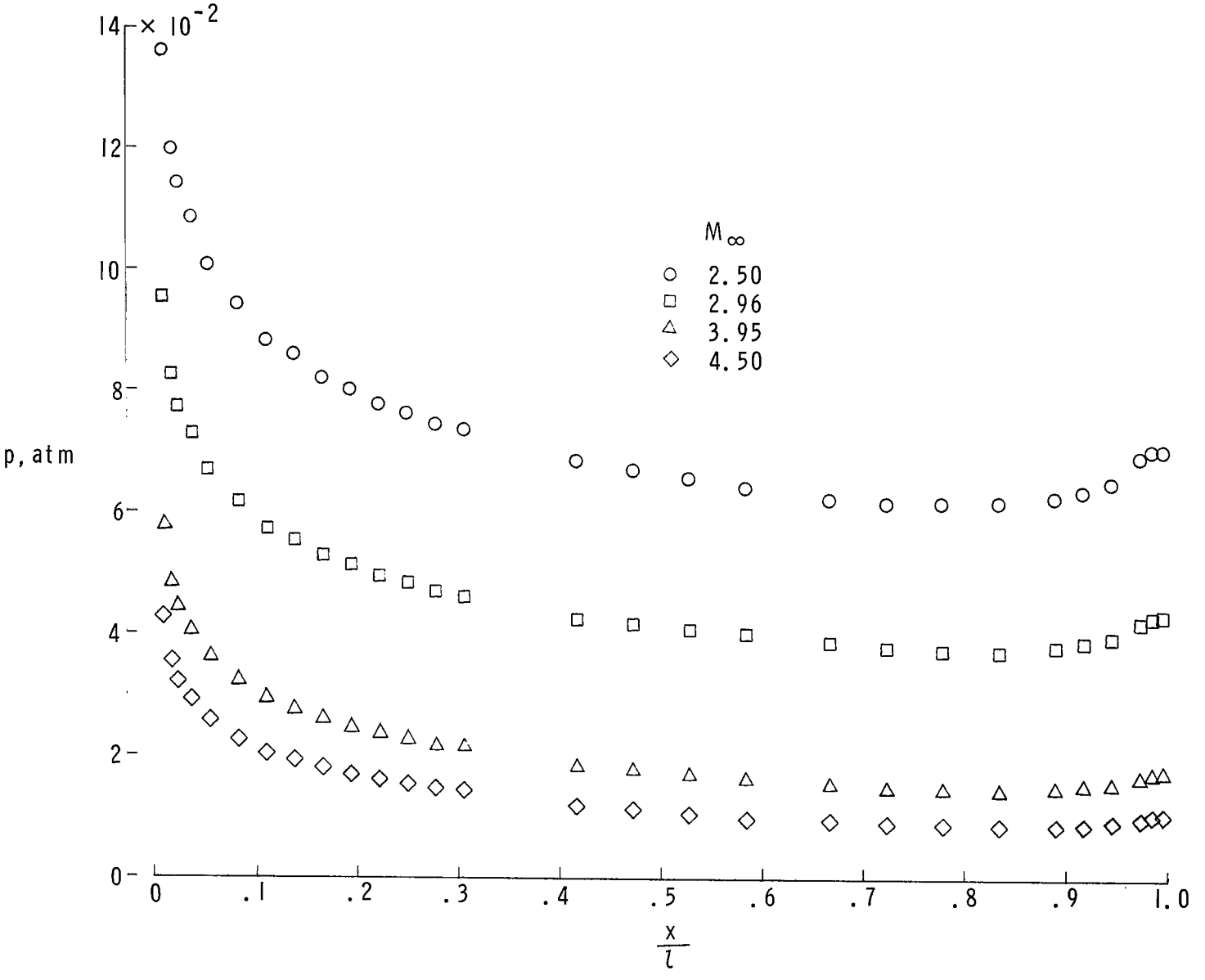

Figure 2.- Static-pressure distributions on Haack-Adams body.

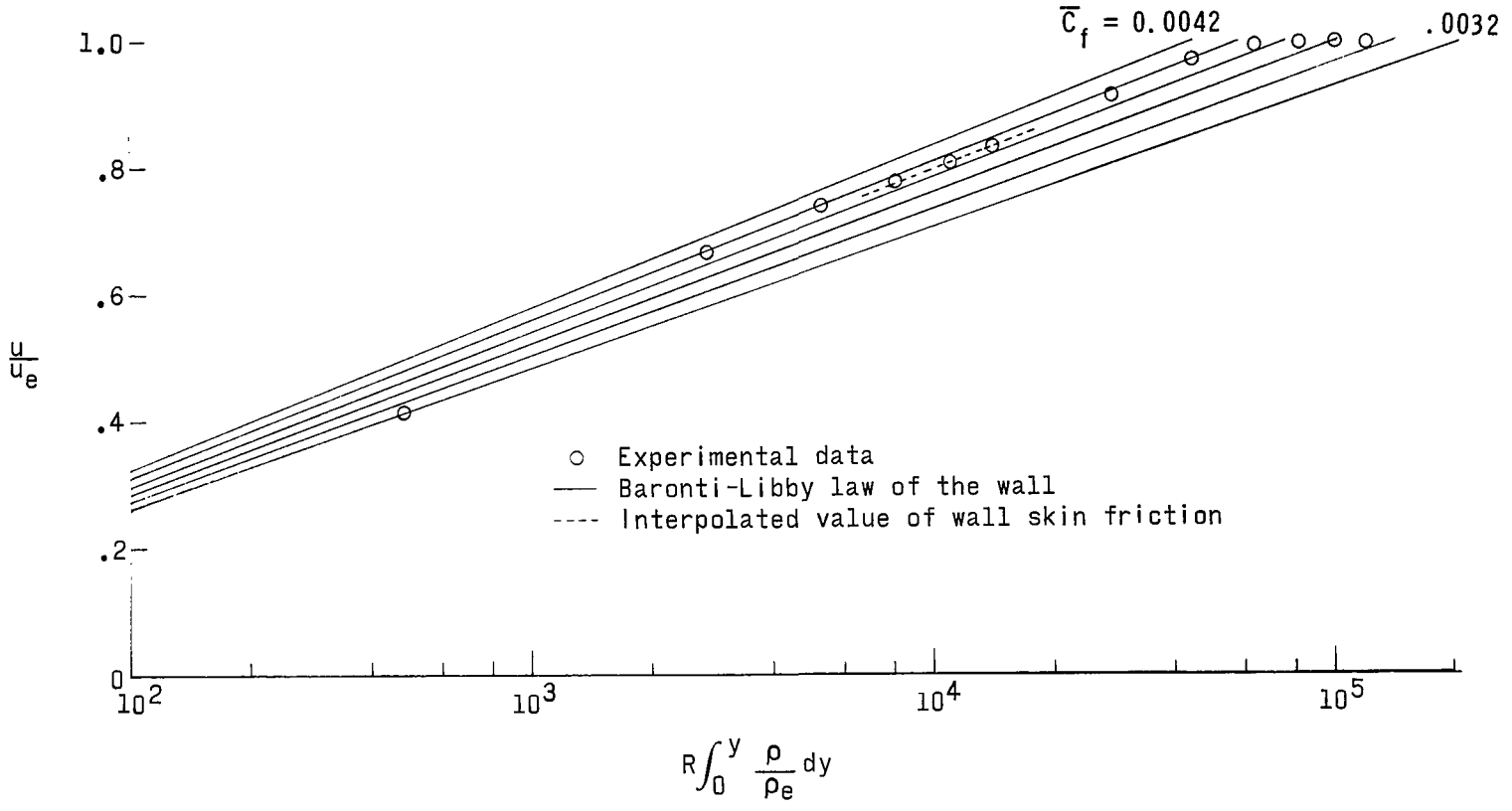

Figure 3.- Law-of-the-wall interpolation technique with experimental velocity profile obtained at station 5. $M_\infty = 2.96$. ($\overline{C}_f$ increment between curves is 0.0002.)

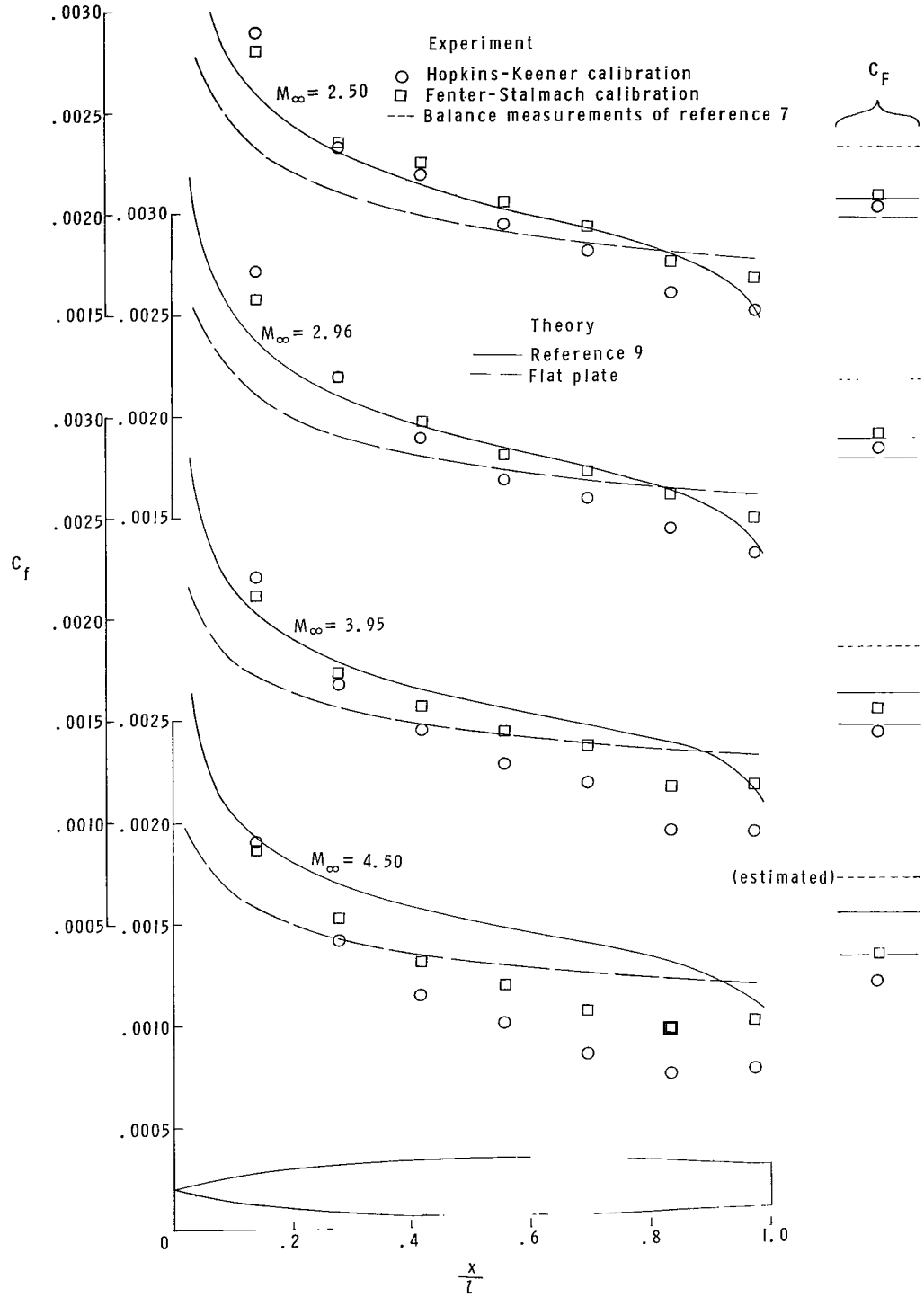

Figure 4.- Preston tube surveys on Haack-Adams body.

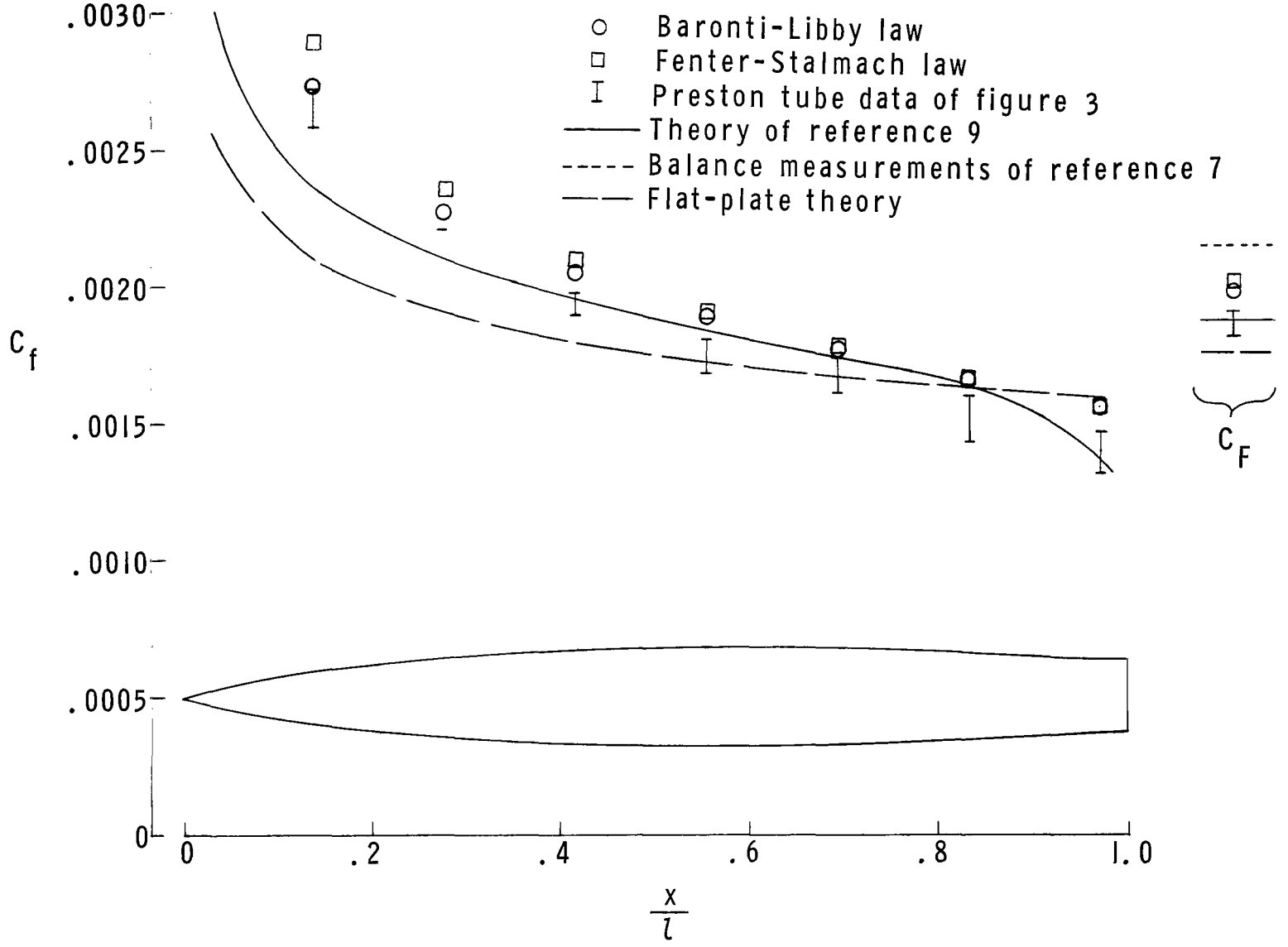

Figure 5.- Law-of-the-wall results on Haack-Adams body. $M_\infty = 2.96$.

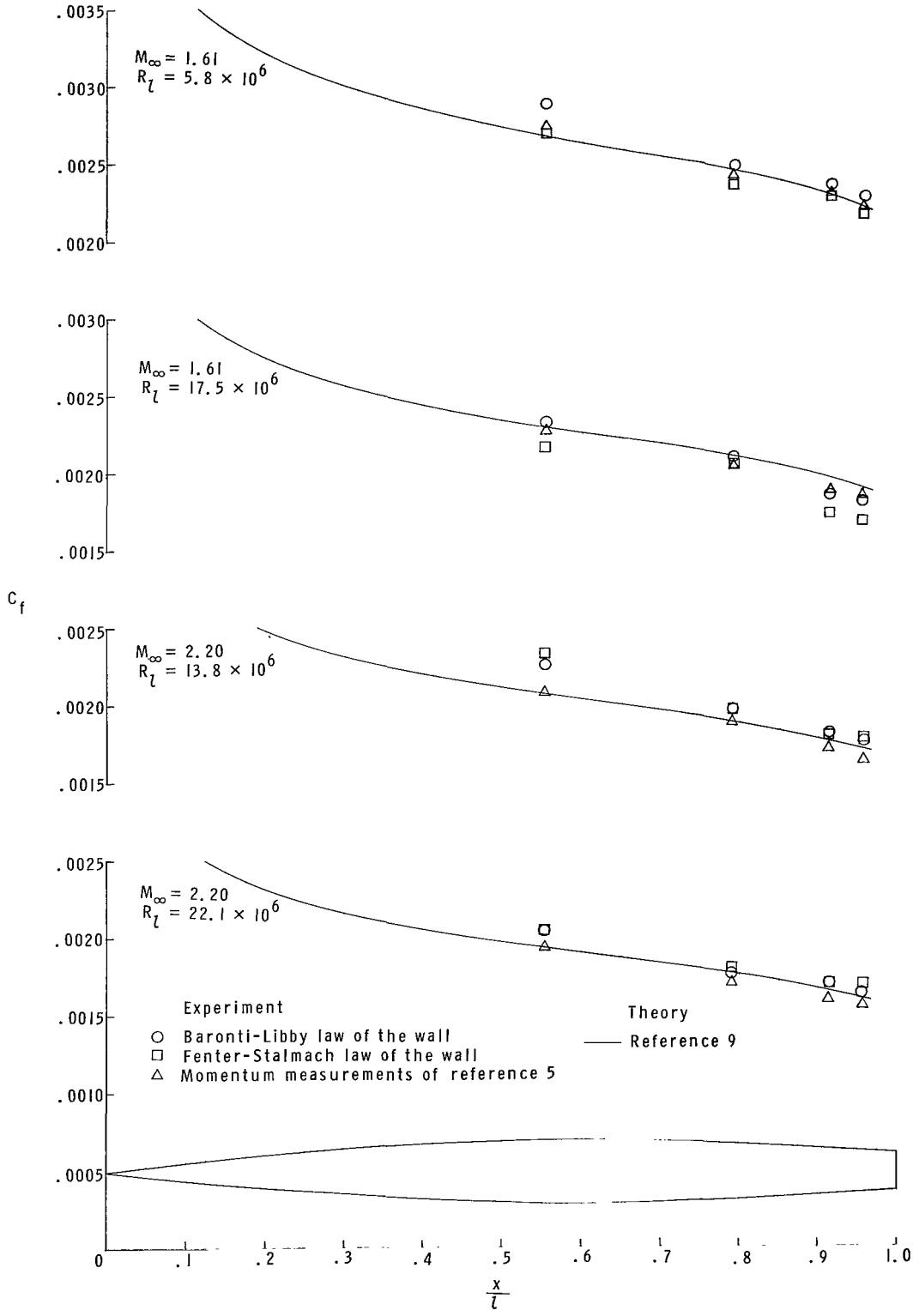

Figure 6.- Law-of-the-wall results on NACA RM-10.

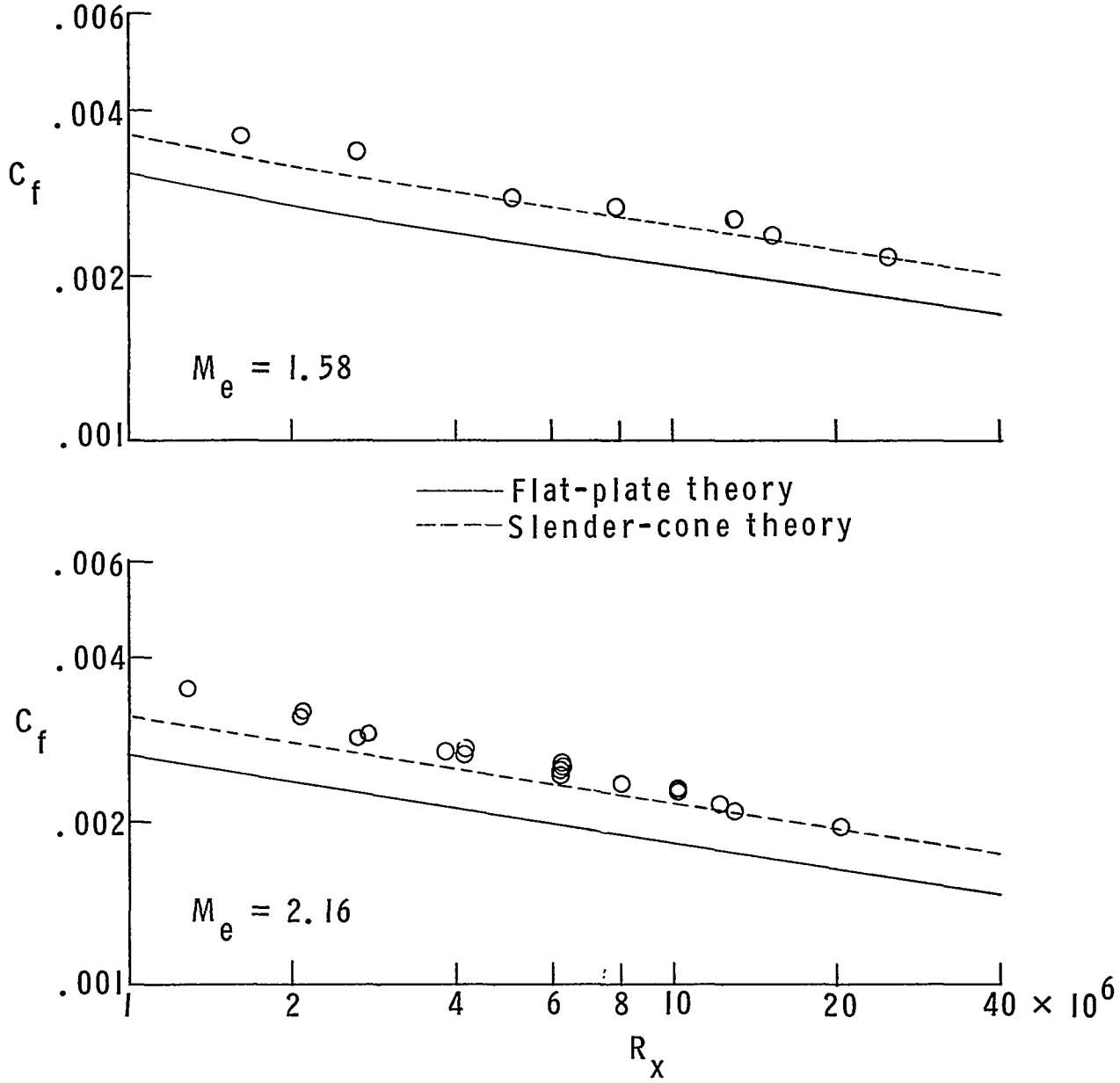

(a) Baronti-Libby law of the wall.

Figure 7.- Slender-cone results.

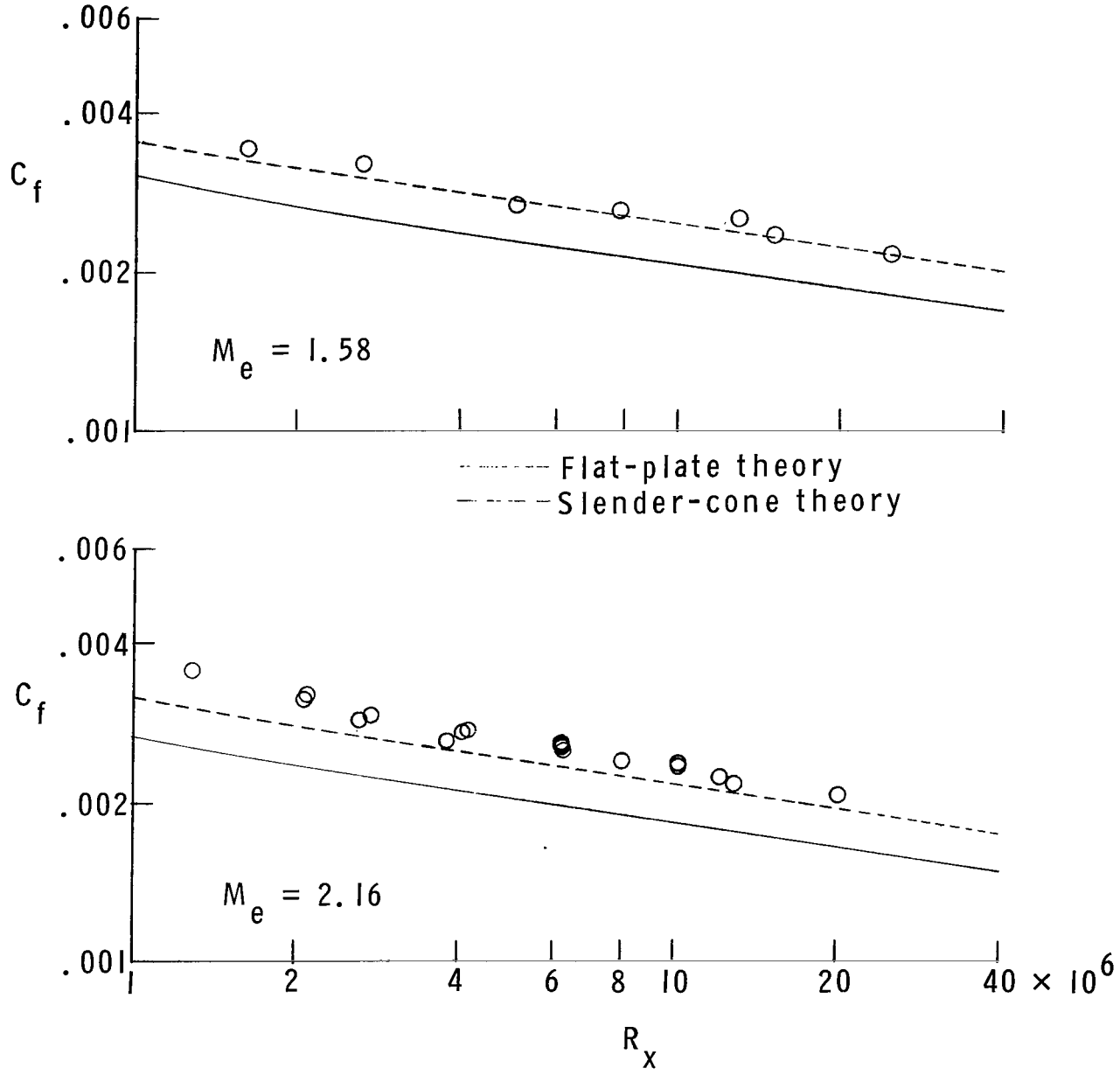

(b) Fenter-Stalmach law of the wall.

Figure 7.- Continued.

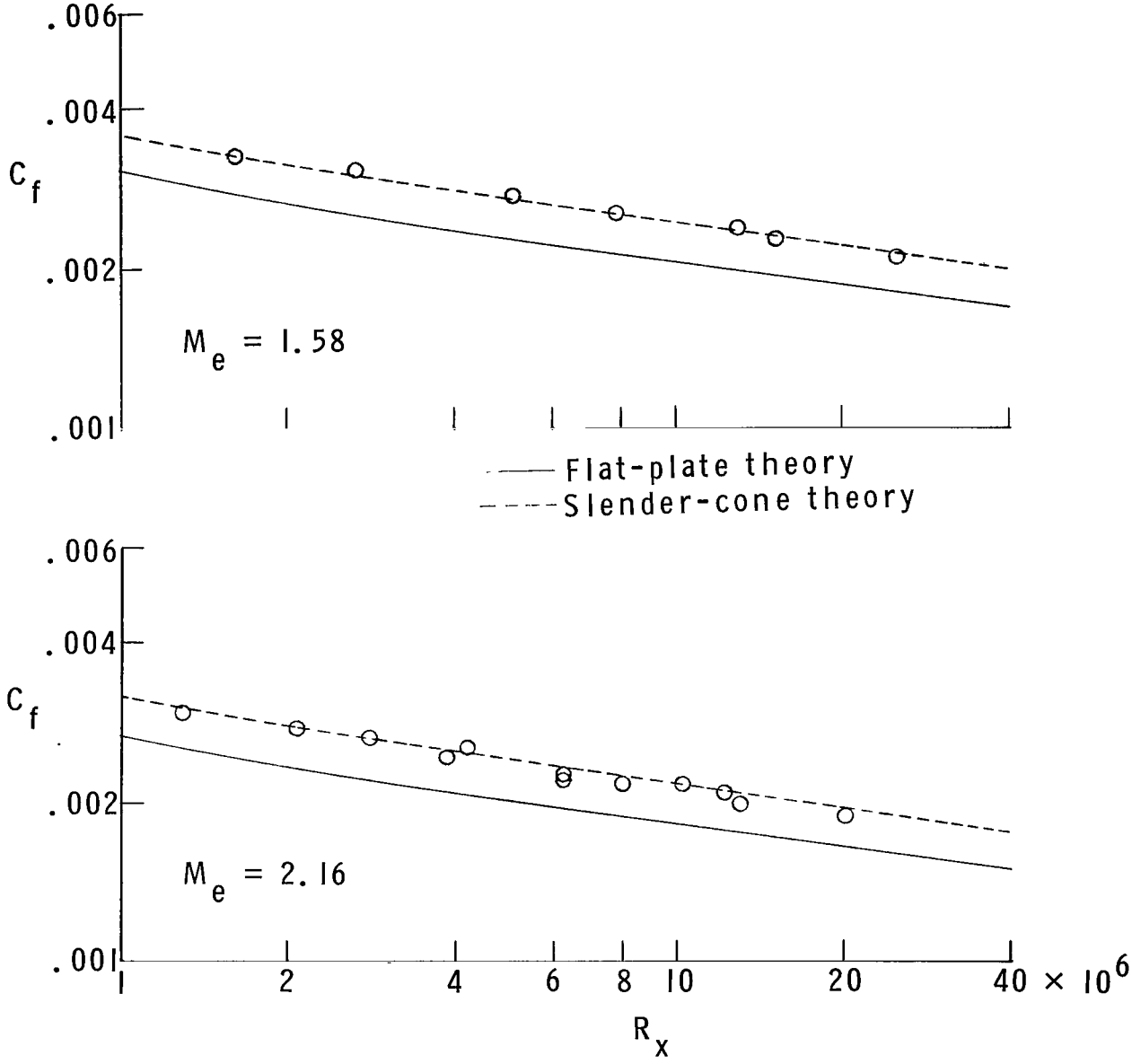

(c) Momentum-thickness measurements of reference 5.

Figure 7.- Concluded.

"The aeronautical and space activities of the United States shall be conducted so as to contribute . . . to the expansion of human knowledge of phenomena in the atmosphere and space. The Administration shall provide for the widest practicable and appropriate dissemination of information concerning its activities and the results thereof."

—NATIONAL AERONAUTICS AND SPACE ACT OF 1958

NASA SCIENTIFIC AND TECHNICAL PUBLICATIONS

TECHNICAL REPORTS: Scientific and technical information considered important, complete, and a lasting contribution to existing knowledge.

TECHNICAL NOTES: Information less broad in scope but nevertheless of importance as a contribution to existing knowledge.

TECHNICAL MEMORANDUMS: Information receiving limited distribution because of preliminary data, security classification, or other reasons.

CONTRACTOR REPORTS: Scientific and technical information generated under a NASA contract or grant and considered an important contribution to existing knowledge.

TECHNICAL TRANSLATIONS: Information published in a foreign language considered to merit NASA distribution in English.

SPECIAL PUBLICATIONS: Information derived from or of value to NASA activities. Publications include conference proceedings, monographs, data compilations, handbooks, sourcebooks, and special bibliographies.

TECHNOLOGY UTILIZATION PUBLICATIONS: Information on technology used by NASA that may be of particular interest in commercial and other non-aerospace applications. Publications include Tech Briefs, Technology Utilization Reports and Notes, and Technology Surveys.

Details on the availability of these publications may be obtained from:

SCIENTIFIC AND TECHNICAL INFORMATION DIVISION

NATIONAL AERONAUTICS AND SPACE ADMINISTRATION

Washington, D.C. 20546